Journal of Inorganic and Organometallic Polymers and Materials (2021) 31:1668–1675
https://doi.org/10.1007/s10904-020-01798-x

A Compare Study on Electrical Properties of MS Diodes with and Without $CoFe_2O_4$-PVP Interlayer

A. Tataroglu[1] · A. Buyukbas Ulusan[1] · Ş. Altındal[1] · Y. Azizian-Kalandaragh[2,3]

Received: 30 August 2020 / Accepted: 19 October 2020 / Published online: 26 October 2020

Abstract
Cobalt ferrite ($CoFe_2O_4$) nanostructures in powder form were synthesized by an ultrasound assisted method. The crystalline structure of it was determined by XRD method. The prepared powder was mixed with an aqueous polyvinylpyrrolidone (PVP) solution to utilize as an interfacial thin film. The prepared $CoFe_2O_4$-PVP solution was deposited on the n-Si wafer utilizing electrospinning method. Electrical characteristics of the Au/n-Si (MS) and Au/($CoFe_2O_4$-PVP)/n-Si (MPS) diodes were investigated using current and admittance ($Y = G + i\omega C$) measurements. Electrical parameters like ideality factor (n), barrier height (Φ_B), and series resistance (R_s) of them were extracted from I–V measurements. The $Ln(I_F)$-(V_F) plots were drawn to determine the current conduction mechanisms (CCMs). Besides, the other diode parameters including diffusion potential, concentration of donor atoms, depletion layer width, barrier height and Fermi-energy were extracted from C^{-2}–V characteristic. As a result, the electrical parameters of these diodes were compared with each other, and the obtained results confirm that the polymer interlayer between M and S is more affective on electrical performance of the diode.

Keywords Cobalt ferrite ($CoFe_2O_4$) · Polyvinylpyrrolidone (PVP) · MS and MPS diode · Current conduction mechanisms · Electronic parameters

1 Introduction

A metal-polymer-semiconductor (MPS) structure is made by sandwiching a polymer/organic film between M and S. The electrical and dielectric behaviors of MPS structure are almost identical those of devices such as MIS and MOS devices [1–5]. As with Schottky barrier diode (SBD), MPS device indicates rectifier behavior. Polymer thin films as gate insulators are often used in different devices like batteries, solar cells, transistors, sensors and light-emitting diodes. Polymers obtained by simple solution techniques are highly attractive for these devices. Polymers like polyvinyl-pyrrolidone (PVP), polyvinyl alcohol (PVA), polyaniline (PANI) and polypyrrole (PPy) are another group of vinyl polymer. Polymer thin films can be prepared using various techniques such as drop-coating, dip-coating, ink printing, spraying, electrospinning, and spin coating [6–8]. Electrospinning and spin coating technique is one of the important techniques used to obtain high quality polymer thin films. Polyvinylpyrrolidone (PVP) is a highly polar and an amorphous polymer. PVP has important and useful properties like good easy processability, very low toxicity, high water solubility, good film-forming, good thermal and mechanical stability [8–11]. PVP is also used in ceramic, electrical, metallurgical, and pharmaceutical industry, various cosmetics, adhesives, and coatings.

Cobalt-ferrite ($CoFe_2O_4$) is a spinel ferrite such as $MgFe_2O_4$, $MnFe_2O_4$, and $ZnFe_2O_4$. Among these ferrites, the cobalt ferrite has excellent physical and chemical properties like good stability, high coercivity, good mechanical hardness, strong anisotropy, and moderate saturation magnetization [12–19]. It has a cubic spinel structure and is a magnetic material. The cobalt ferrite is used in various applications digital recording disks, storage devices, magnetic and switching devices, transformers, audio, and videotape.

In the present work, the electrospinning method was used for the deposition of polymer thin film on n-Si wafer. Then,

✉ A. Tataroglu
ademt@gazi.edu.tr

[1] Physics Department, Faculty of Sciences, Gazi University, Ankara, Turkey

[2] Department of Physics, University of Mohaghegh Ardabili, P.O. Box 179, Ardabil, Iran

[3] Department of Engineering Sciences, Sabalan University of Advanced Technologies (SUAT), Namin, Iran

the MS diodes with and without $CoFe_2O_4$-PVP interlayer were prepared by forming ohmic and rectifier contacts. The main electronic parameters of them were calculated by using various methods such as Thermionic Emission (TE) and Norde.

2 Experimental

2.1 Preparation of $CoFe_2O_4$ Nanostructures

For preparation of $CoFe_2O_4$ nanostructures, 0.1 M of cobalt acetate (from Loba Chemie Company) was dissolved in deionize-water (DW) as cobalt source and in another backer, 0.1 M of Iron chloride ($FeCl_2$) was dissolved in the same procedure in double distilled water, both of anionic and cationic precursors were mixed in a rounded bottom backer and kept under ultrasonic waves for 15 min, the ultrasonic irradiation was not continued process. Every 5 min, the ultrasonic process was stopped for 5 min. After that, the prepared suspension was centrifuged and washed with distilled water for several times, and eventually, the material dried in the open air, and then the as-utilized powder was annealed in an ordering oven for 60 min and then it was characterized by XRD.

2.2 The Fabrication Process of MS and MPS Diodes

To fabricate the MS diodes with and without $CoFe_2O_4$-PVP interlayer, the n-Si wafer having (100) orientation and resistivity of 1–10 Ωcm is used. Firstly, it was dipped in ammonium-peroxide ($(NH_4)_2O_2$) to remove organic contamination and native oxide on the surface of wafer and then it is etched using various acidic and basic chemical solutions. The chemically cleaned wafer is rinsed in ultra-pure deionized water and dried with pure-N_2 gas. Consequently, ohmic and rectifier contacts to be used for electricity transmission were formed. For ohmic contact with about 1500 Å thickness, high-pure Au was grown as thermally onto back-side of wafer at 10^{-6} Torr and then the wafer was annealed at 550 °C for 5 min under N_2 atmosphere. For rectifier contact with about 1500 Å thickness, Au rectifier contacts with 1 mm diameter were grown on the first quarter of the wafer. Thus, Au/n-Si (MS) diode was completed. To grow the ($CoFe_2O_4$-PVP) interlayer on the second quarter wafer, electrospinning method was used and then the same Au rectifier contacts were grown on the interlayer. Thus, Au/($CoFe_2O_4$-PVP)/n-Si (MPS) diode was fabricated. The I–V and C/G–V measurements were carried out by using Keithley 2400 and HP 4192A LF, respectively.

3 Result and Discussion

3.1 $CoFe_2O_4$ Nanostructure Analysis

Figure 1 shows the XRD pattern of the prepared powders, which depicted cubic $CoFe_2O_4$ crystalline structure. The broadness of the peaks confirms the nano-dimension of the product. There are no other peaks in the pattern, and it shows the purity of $CoFe_2O_4$ nanostructures.

Figure 2a and b show field emission scanning electron microscopy (FE-SEM) images of the nanostructures with different magnifications. The morphology of the nanostructures is semi-plate and has a formed in the form of polydispersive cluster nanostructures of less than micron size. For

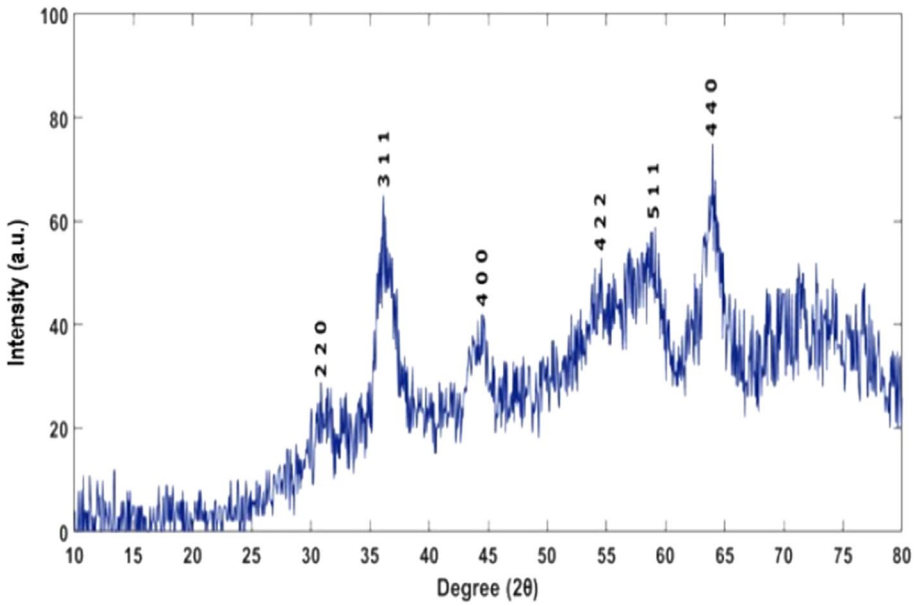

Fig. 1 XRD pattern of $CoFe_2O_4$ nanostructures

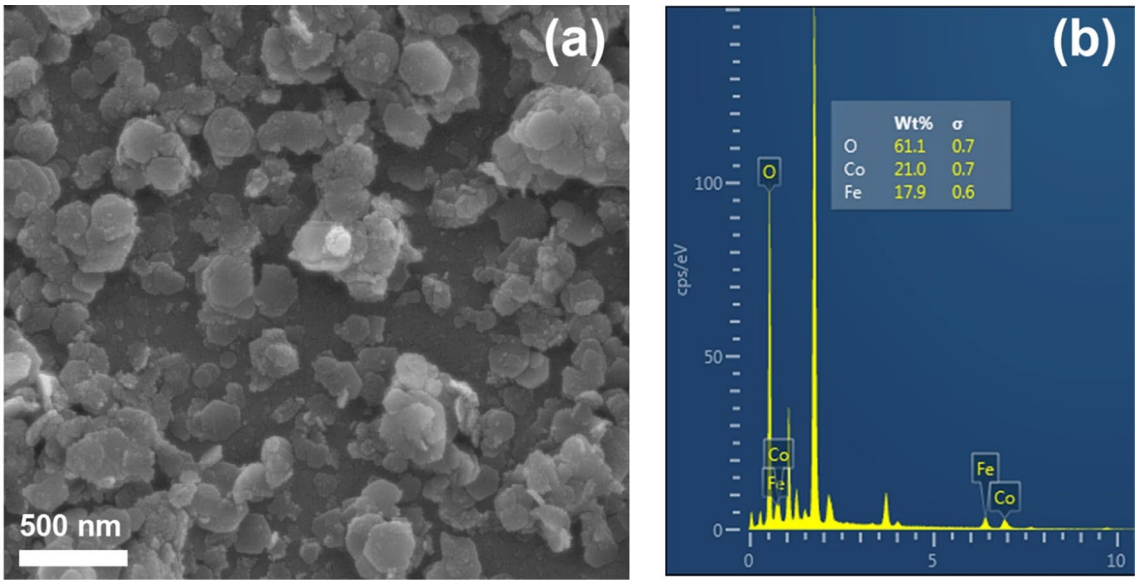

Fig. 2 FE-SEM image in different magnifications. **a** 70 kx, **b** EDX profiles of $CoFe_2O_4$ nanostructures

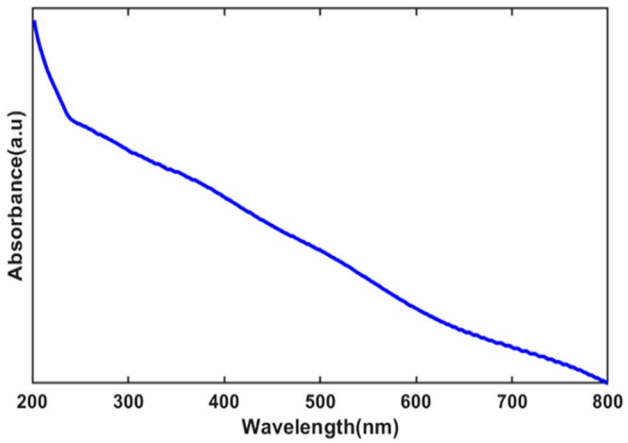

Fig. 3 UV–Vis absorption spectra for $CoFe_2O_4$ nanostructures

the chemical characterization of $CoFe_2O_4$ nanostructures, the energy dispersive X-ray (EDX) analysis was used to recognize the presented elements in the prepared Nano powder. The results of the EDX analysis are shown in Fig. 2b. The observed a sharp peak of Oxygen(O) with a weight percentage of 61.1, Cobalt (Co) with a weight percentage of 21.0 is detected together with the peak of Ferrite (Fe) with a content of 17.9 wt%.

Optical properties of prepared nanostructures were analyzed in the range of 200–800 nm. Optical absorption was used to evaluate the energy gap of the nanostructures shown in Fig. 3. As can be seen from Fig. 3, the nanostructures have low absorbance in the visible regions and high absorbance in the ultraviolet region.

3.2 I-V Characteristics of the MS and MPS Diodes

The conventional I_F-V_F method was used to extract basic diode parameters like saturation current (I_o), ideality factor (n) and barrier height (Φ_{B0}) of the fabricated MS diode with/without ($CoFe_2O_4$-PVP) interlayer. These diodes obeying the TE theory ($V \geq 3kT/q$) is described by the following relations [20, 21],

$$I = I_o\left(\exp\left(\frac{q\left(V - IR_s\right)}{nkT}\right) - 1\right) \tag{1}$$

Both the values of I_o and n are extracted from the intercept and slope of the linear part of the semi-logarithmic I_F-V_F plot, and they are given as follows, respectively,

$$I_o = AA^*T^2\exp\left(-\frac{q\phi_{B0}}{kT}\right) \tag{2}$$

$$n = \frac{q}{kT}\left(\frac{dV}{d(\mathrm{In}I)}\right) \tag{3}$$

Thus, Φ_{B0} value can be obtained from the Eq. (2).

Figure 4 illustrates $Ln(I_F)$-V_F curves of the MS and MPS diodes and the fabricated devices show diode-like behavior. It is clear that I–V curves of these diodes indicate a strongly rectifying behavior. The rectifying-rate (RR) which is the ratio of the current for positive and negative voltage, of the MS and MPS diodes was found as 6.44×10^2 and 3.43×10^3 at ± 3, respectively. As a result, the used ($CoFe_2O_4$-PVP) interlayer leads to the increase RR value.

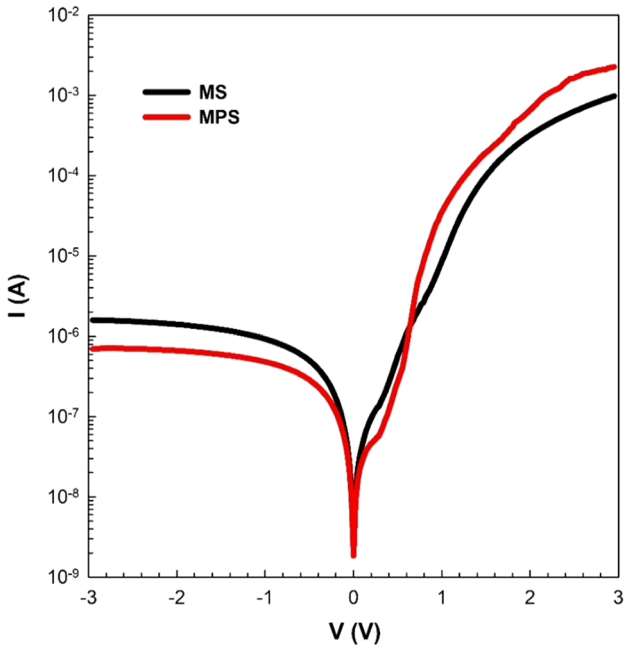

Fig. 4 The $Ln(I_F)$-V_F curves of these diodes

At low voltage, $Ln(I_F)$-V_F curves exhibit a linear behavior. The obtained I_0, n and Φ_{B0} values of the MS and MPS diodes are presented in Table 1. It is seen that the obtained n and Φ_{B0} value of MPS is higher than MS diode. This result is due to the $CoFe_2O_4$-PVP interlayer. Besides, the obtained n value has greater than unity. For an ideal Schottky diode with current-dominated by TE, the n value must be equal to unity. The obtained high values of n can be caused by the R_s, non-homogeneous barrier, tunneling-current, existence of interlayer and N_{ss} [20–28]. In addition, at higher voltages, the I–V curves deviate from linearity due to the R_s.

To obtain the values of series resistance and shunt resistance (R_{sh}) of these diodes, Ohm's law ($R_j = \partial V/\partial I$) was used. Figure 5 illustrates the diode-resistance (R_j)-V curves of these diodes. Since the R_j-V curve becomes almost constant value for the high-reverse biases, the calculated value corresponds to the R_{sh} and it was found to be 1.90 MΩ and 4.47 MΩ at − 3 V for MS and MPS diode, respectively. If the R_j-V curve shows almost constant value in the forward bias region, the calculated value corresponds to the R_s. The R_s values were found to be 2.95 kΩ and 1.30 kΩ at + 3 V, respectively.

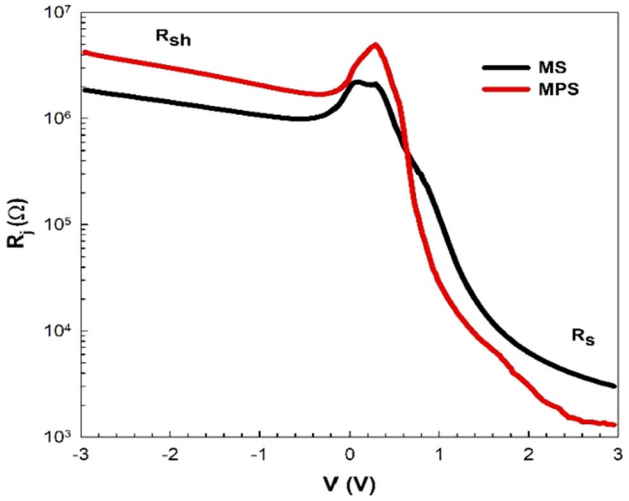

Fig. 5 The R_j-V curves of these diodes

After determining the n and Φ_{B0} from the I–V characteristic using TE theory, Norde method was used as another approach to extract the Φ_B and R_s [29]. In this approach, Norde function, F(V), is given as:

$$F(V) = \frac{V}{\gamma} - \frac{kT}{q}\left[\ln\left(\frac{I(V)}{AA^*T^2}\right)\right] \tag{4}$$

In Eq. 4, γ is an integer greater than n value. Accordingly, the Φ_B and R_s are given as follows,

$$\Phi_B = F\left(V_{min}\right) + \frac{V_{min}}{\gamma} - \frac{kT}{q} \tag{5}$$

$$R_s = \frac{kT(\gamma - n)}{qI_{min}} \tag{6}$$

This method includes F(V) plotted against voltage (V). This plot must give a distinctive minimum point, $F(V_{min})$. V_{min} and I_{min} are voltage and current values corresponding the $F(V_{min})$, respectively. Figure 6 shows F–V curves of these diodes. It is observed that these plots has a minimum point. The extracted Φ_B and R_s values are also tabulated in Table 1 and the value of BH obtained from Norde and TE theory are in good agreement with each other.

Table 1 The determined electronic parameters of these diodes

Diode	I_0 (A) (TE)	n (TE)	Φ_{b0} (eV) (TE)	Φ_b (eV) (Norde)	R_s (Ω) (Norde)	R_{sh} (MΩ) (Ohm's Law)
MS	1.38×10^{-8}	3.43	0.76	0.78	3.93×10^{5}	1.90
MPS	9.23×10^{-9}	4.41	0.77	0.79	6.41×10^{5}	4.47

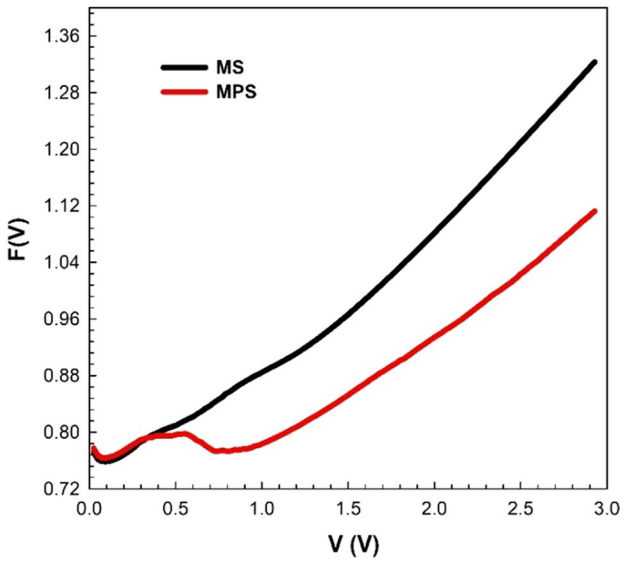

Fig. 6 F(V)-V curves of these diodes

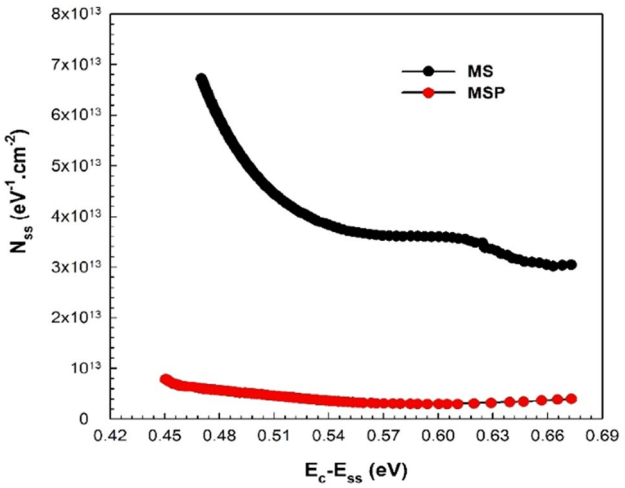

Fig. 7 The energy distribution curves of N_{ss} for these diodes

To extract the density of N_{ss} for two type diodes, the approach proposed by Card and Rhoderick [30] was used. In this method, the energy distribution profile of N_{ss} is obtained with the help of the I_F-V_F characteristics. The unit of N_{ss} is $eV^{-1}.cm^{-2}$, and the N_{ss} is given as,

$$N_{ss}(V) = \frac{1}{q}\left[\frac{\varepsilon_i}{\delta}(n(V)-1) - \frac{\varepsilon_s}{W_D}\right] \tag{7}$$

In this equation, δ and W_D are the interlayer thickness and depletion layer width determined from C^{-2}–V curve as following section, respectively. Besides, ε_i and ε_s are the permittivity of the interlayer and semiconductor, respectively. The conduction band edge energy (E_c) with respect to the surface state energy (E_{ss}) for n-type semiconductor is given by [21, 30],

$$E_c - E_{ss} = q\left(\Phi_e - V\right) \tag{8}$$

where Φ_e is the effective BH (ϕ_e) and is given as follows,

$$\Phi_e - \Phi_{B0} = \left(1 - \frac{1}{n(V)}\right)\left(V - IR_s\right) \tag{9}$$

Figure 7 shows the N_{ss} vs (E_c-E_{ss}) of the MS and MPS diodes. For MS and MPS diodes, the N_{ss} values at about $E_c = 0.47$ eV are found to be 6.72×10^{13} eV^{-1} cm^{-2} and 6.24×10^{12} eV^{-1} cm^{-2}, respectively. As can be seen in Fig. 7, N_{ss} value of MPS diode is lower than the MS diode. This results from the passivated role of the interfacial layer or the saturation of dangling- bonds [31–33].

In addition, the In(I_F)-Ln(V_F) plots were drawn to determine the current (CMs) for the two diodes, and represented in Fig. 8 and these curves were indicated three linear regions called as Region 1, 2, and 3 that obeys I α V^m relation. The m values were calculated from the slope of In(I_F)-V_F curves. For the three regions, the m values of MS diode were found to be 1.17, 3.89 and 4.11, respectively. For MPS diode, the m values were found to be 1.04, 7.56 and 4.16.

In the Region 1, the obtained m value for two diodes is close to unity. This result indicates that the CCM of these diodes exhibits an ohmic behavior. In other words, the CM is governed by Ohm's law. In the Region 2, the obtained m value is larger than 2. This case shows that the CCM or current transport is governed by trap-charge limited current (TCLC) with an exponential trap distribution. In the

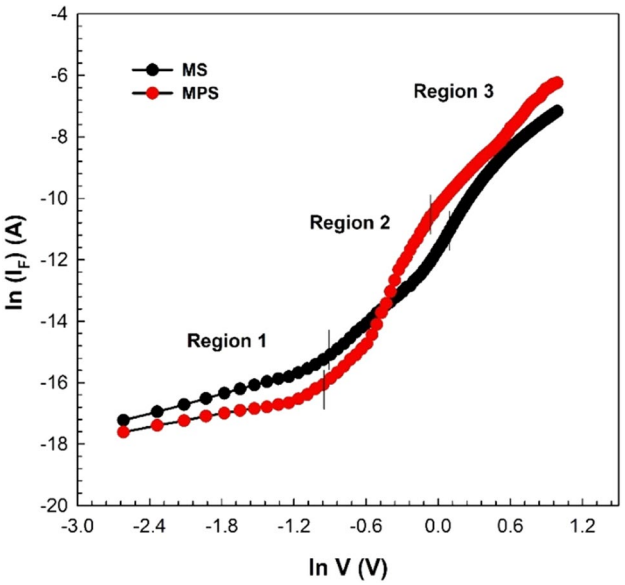

Fig. 8 The double-logarithmic I_F-V_F curves of these diodes

Region 3, the dominant CCM is space charge limited current (SCLC) controlled by single dominating trap-level [34–38].

3.3 C-V and G/ω-V Characteristics of the MS and MPS Diodes

Both capacitance and conductance measurements were performed at wide range of bias voltages between − 2 V and + 4 V and 1 MHz. The surface states cannot follow the frequency of the ac signal and hence cannot any contribution the measured of them at high frequencies (f ≥ 500 kHz). Therefore, they cannot contribute to total capacitance [3, 20, 39–44]. Figure 9a and b demonstrate the C–V and G/ω-V plots of these diodes at 1 MHz, respectively. As seen in Fig. 9, the capacitance and conductance indicate a strong dependence on voltage. Also, the C value of MS diode is higher than MPS diode. This case is due to the interlayer, which causes a decrease in interface states.

Another technique for measuring series resistance (R_s) is the admittance method developed by Nicollian and Goetzberger and according to this method, R_s can be calculated as follow [45].

$$R_s = \frac{G_{ma}}{G_{ma}^2 + \left(\omega C_{ma}\right)^2} \tag{10}$$

In Eq. 10, G_{ma} and C_{ma} represent the measured values of them at accumulation region, respectively. Figure 10 shows the plots of R_s-V of these diodes at 1 MHz, which has a peak at about 0.5 V. This peak is due to a special distribution

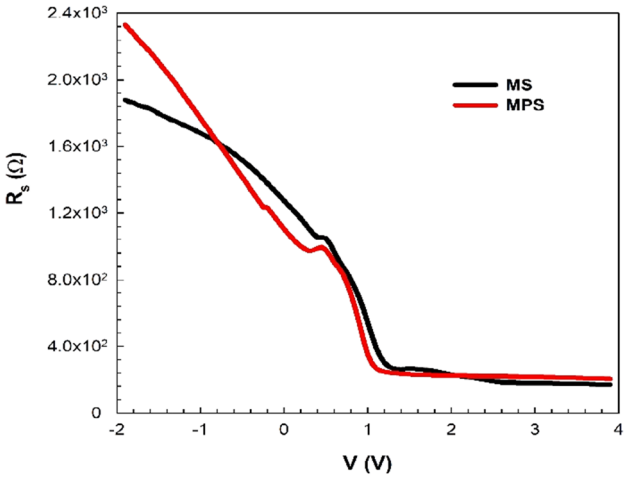

Fig. 10 R_s-V plots of these diodes

of N_{ss} located at ($CoFe_2O_4$-PVP)/n-Si interface and their relaxation or life time.

The values of Fermi-energy (E_F), concentration of donor atoms (N_D), diffusion-potential ($V_D = V_0 + kT/q$), W_D and Φ_B(C–V) of these diodes can be calculated from the C^{-2}–V characteristic given in Fig. 11. The relation between capacitance and V is given as follows [20, 21, 46–53],

$$C^{-2} = 2\left(V_o + V\right)/\left(q\varepsilon_s\varepsilon_o A^2 N_D\right) \tag{11}$$

The value of V_0 and N_D was extracted from the intercept and slope of the linear region of C^{-2}–V plot. Other parameters given below were calculated using the V_0 and N_D values.

$$E_F = \frac{kT}{q}\mathrm{In}\left(\frac{N_C}{N_D}\right),\ E_m = \left[\frac{2qN_DV_0}{\varepsilon_s\varepsilon_0}\right]^{0.5},\ \Delta\Phi_b = \left[\frac{qE_m}{4\pi\varepsilon_s\varepsilon_0}\right]^{0.5} \text{and } W_D = \sqrt{\frac{2\varepsilon_s\varepsilon_0V_D}{qN_D}} \tag{12}$$

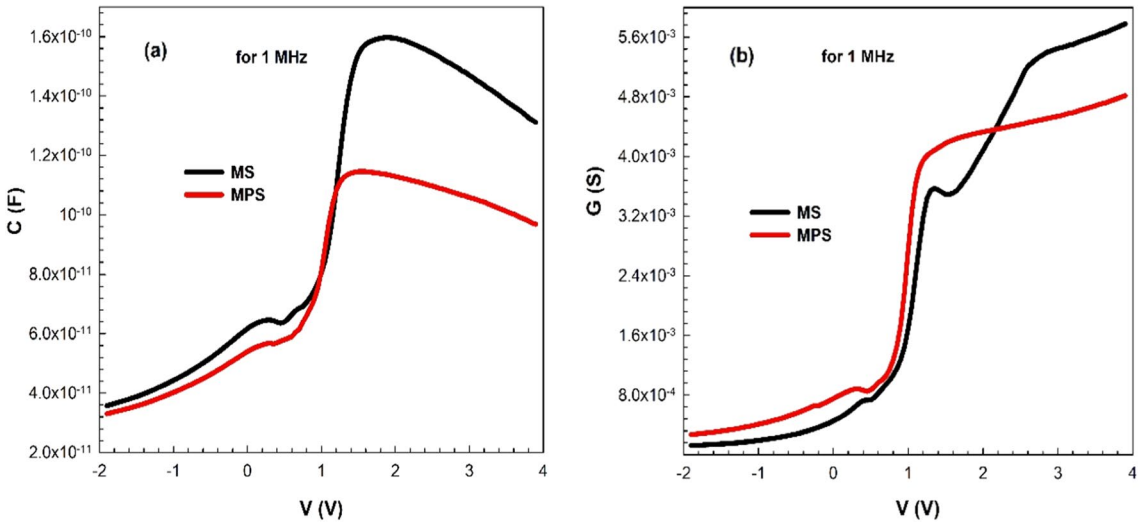

Fig. 9 Plots of **a** C–V and **b** G/ω-V of these diodes at 1 MHz

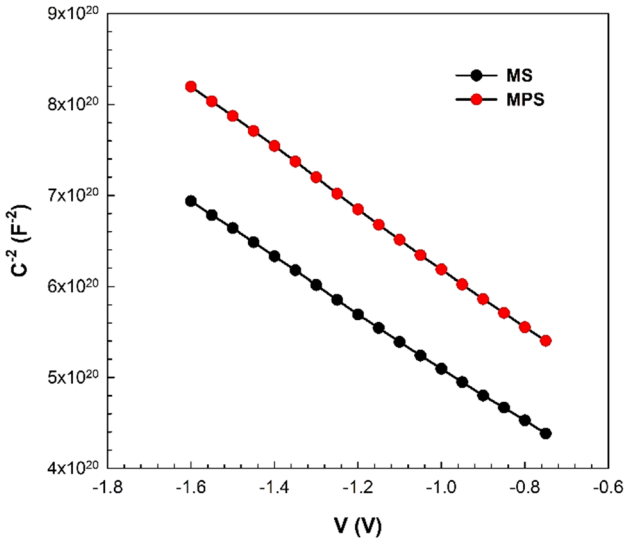

Fig. 11 The C^{-2}–V plots of these diodes at 1 MHz

Thus, the $\Phi_{B(C\text{-}V)}$ can be calculated as follows,

$$\Phi_{B(C-V)} = V_D + \frac{kT}{q}\ln\left(\frac{N_C}{N_D}\right) - \Delta\Phi_B = V_D + E_F - \Delta\Phi_B \tag{13}$$

It is seen that these plots exhibit a good linear behavior in the inversion region. The calculated parameters are given in Table 2, and Φ_B value of the MPS is higher than the MS diode. This is due to the existence of the ($CoFe_2O_4$-PVP) interlayer.

4 Conclusions

In this study, both the MS and MPS diodes were prepared on the same n-Si wafer to investigate the effects of ($CoFe_2O_4$-PVP) interlayer on the electrical characteristics by using I–V and C–V measurements. The values of I_0, n and Φ_{B0} of these diodes were extracted from both TE and Norde methods. The observed a deviation from the linearity in $Ln(I_F)$-V_F and concave curvature in C–V curves at adequate high forward voltages was explained on the basis of R_s and native SiO_2 and ($CoFe_2O_4$-PVP) interlayers because of the sharing of applied voltage by depletion layer, R_s, and interlayer. Also, the current conduction mechanisms of these diodes were investigated from the $\ln(I_F)$-$\ln(V_F)$ which are obey $I\alpha V^m$ relation. Additionally, the RR value for MS and MPS diodes was found as 6.44×10^2 for MS and 3.43×10^3 for MPS diode at ±3,, respectively. The high value of the MPS diode is the result of the $CoFe_2O_4$-PVP interlayer. Similarly, the magnitude of N_{ss} for MS and MPS diodes was found as 6.72×10^{13} eV^{-1} cm^{-2} and 6.24×10^{12} eV^{-1} cm^{-2}, respectively. The low value of the MPS diode is caused by the passivation effect of interface states. The C–V and G/ω measurements indicate that both the C and G are dependent of voltage and interlayer. In addition, other electronic parameters of these diodes were determined from the C^{-2}–V characteristics. The obtained results show that the interlayer, N_{ss} and R_s can cause to significant effects both on the electrical characteristics of these MS and MPS diodes.

Table 2 The electrical parameters extracted from the C^{-2}-V characteristics

Electrical parameters	V_D (V)	N_D (cm^{-3})	E_F (eV)	E_m (V/cm)	$\Delta\Phi_B$ (eV)	$\Phi_{B(C\text{-}V)}$ (eV)	W_D (cm)
MS	0.71	6.41×10^{14}	0.245	1.18×10^4	1.20×10^{-2}	0.95	1.20×10^{-4}
MPS	0.87	5.81×10^{14}	0.248	1.24×10^4	1.23×10^{-2}	1.10	1.40×10^{-4}

Acknowledgements This study was supported by Gazi University Scientific Research Project (Project Number: GU-BAP.05/2019-26).

References

1. A. Tataroglu, Ş Altındal, Y. Azizian-Kalandaragh, Phys. B **576**, 411733 (2020)
2. Ş Altındal, Ö. Sevgili, Y. Azizian-Kalandaragh, J. Mater. Sci. **30**, 9273–9280 (2019)
3. M.K. Hudait, S.B. Krupanidhi, Solid-State Electron. **44**, 1089–1097 (2000)
4. V. Rajagopal Reddy, C. Venkata Prasad, K. Ravindranatha Reddy, Solid State Sci. **97**, 105987 (2019)
5. M. Chybicki, Phys. Stat. Sol. (a) **39**, 271–279 (1977)
6. T. Blythe, D. Bloor, *Electrical Properties of Polymers*, 2nd edn. (Cambridge University Press, New York, 2005)
7. W. Knoll, R.C. Advincula, *Functional Polymer Films* (Wiley-VCH Verlag, Weinheim, 2011)
8. J.R. Fried, *Polymer Science and Technology*, 3rd edn. (Prentice Hall, New Jersey, 2014)
9. H.M. Ragab, Phys. B **406**, 3759–3767 (2011)
10. Gh. Mohammed, A.M. El Sayed, W.M. Morsi, J. Phys. Chem. Solids **15**, 238–247 (2018)
11. S. Ningaraju, A.P. Gnana Prakash, H.B. Ravikumar, Solid State Ionics **320**, 132–147 (2018)
12. J. Mohapatra, A. Mitra, D. Bahadur, M. Aslam, J. Alloys Compd. **628**, 416–423 (2015)
13. R.P. Moyet, Y. Cardona, P. Vargas, J. Silva, O.N.C. Uwakweh, Mater. Charact. **61**, 1317–1325 (2010)
14. M. Sangmanee, S. Maensiri, Appl. Phys. A **97**, 167–177 (2009)
15. T. Prabhakaran, J. Hemalatha, Ceram. Int. **42**, 14113–14120 (2016)
16. H. Sun, Y. Tang, C.W. Koh, S. Ling, R. Wang, K. Yang, J. Yu, Y. Shi, Y. Wang, H.Y. Woo, X. Guo, Adv. Mater. **31**, 1807220 (2019)
17. Y. Teshima, M. Saito, T. Mikie, K. Komeyama, H. Yoshida, I. Osaka, Bull. Chem. Soc. Jpn. **93**, 561–567 (2020)
18. Y. Jiang, P.K. Upputuri, C. Xie, Z. Zeng, A. Sharma, X. Zhen, J. Li, J. Huang, M. Pramanik, K. Pu, Adv. Mater. **31**, 1808166 (2019)
19. K. Akagi, Bull. Chem. Soc. Jpn. **92**, 1509–1655 (2019)
20. S.M. Sze, *Physics of Semiconductor Devices*, 2nd edn. (Wiley, New York, 1981)
21. E.H. Rhoderick, R.H. Williams, *Metal Semiconductor Contacts*, 2nd edn. (Clarendon Press, Oxford, 1988)
22. A. Büyükbaş Uluşan, A. Tataroğlu, Y. Azizian-Kalandaragh, Ş Altındal, J. Mater. Sci. **29**, 159–170 (2018)
23. V. Rajagopa lReddy, C. Venkata Prasad, Mater. Sci. Eng. B **231**, 74–80 (2018)
24. A. Tataroglu, J. Mater. Electron. Dev. **1**, 6–10 (2017)
25. S. Altındal, J. Mater. Electron. Dev. **1**, 38–43 (2015)
26. F.Z. Pur, A. Tataroglu, Phys. Scr. **86**, 035802 (2012)
27. M. Raj, C. Joseph, M. Subramanian, V. Perumalsamy, V. Elayappan, New J. Chem. **44**, 7708–7718 (2020)
28. A. Kumar, A. Kumar, K.K. Sharma, S. Chand, Superlattices Microstruct. **128**, 373–381 (2019)
29. H. Norde, J. Appl. Phys. **50**, 5052–5054 (1979)
30. H.C. Card, E.H. Rhoderick, J. Phys. D **4**, 1589–1601 (1971)
31. V.R. Reddy, Thin Solid Films **556**, 300–306 (2014)
32. S. Alialy, H. Tecimer, H. Uslu, Ş Altındal, J. Nanomed. Nanotechol. **4**, 1000167 (2013)
33. S. Altındal Yerişkin, M. Balbaşı, İ Orak, J. Mater. Sci. **28**, 14040–14048 (2017)
34. M.A. Lampert, P. Mark, *Current Injection in Solids* (Academic Press, New York, London, 1970)
35. E.A. Akhlaghi, Y. Badali, Ş Altındal, Y. Azizian-Kalandaragh, Phys. B **546**, 93–98 (2018)
36. A. Tataroglu, A.A. Hendi, R.H. Alorainy, F. Yakuphanoglu, Chin. Phys. B **23**, 057504 (2014)
37. A.S. Shikoh, Z.R. Ahmad, F. Touati, R.A. Shakoor, J. Bhadra, N.J. Al-Thani, RSC Adv. **7**, 35445–35450 (2017)
38. V. Rajagopal Reddy, V. Manjunath, V. Janardhanam, Y.-H. Kıl, C.-J. Cho, J. Electron. Mater. **43**, 3499–3907 (2014)
39. E.H. Nicollian, J.R. Brews, *MOS Physics and Technology* (Wiley, New York, 1982)
40. Ç.G. Türk, S.O. Tan, Ş Altındal, B. İnem, Phys. B **582**, 411979 (2020)
41. N. Kaymak, E. Efil, E. Seven, A. Tataroglu, S. Bilge Ocak, E. Orhan, Phys. B **576**, 411721 (2020)
42. F.Z. Acar, A. Buyukbas-Ulusan, A. Tataroglu, J. Mater. Sci. **29**, 12553–12560 (2018)
43. A. Karabulut, A. Dere, O. Dayanc, A.G. Al-Sehemi, Z. Serbetci, A.A. Al-Ghamdi, F. Yakuphanoglu, Mater. Sci. Semicond. Process. **91**, 422–430 (2019)
44. V. Rajagopal Reddy, C.-J. Choi, Vacuum **164**, 233–241 (2019)
45. E.H. Nicollian, A. Goetzberger, Bell Syst. Tech. J. **46**, 1055–1133 (1967)
46. A. Tataroglu, Chin. Phys. B **22**, 068402 (2013)
47. V. Rajagopal Reddy, L. Dasaradha Rao, V. Janardhanam, M.-S. Kang, C.-J. Choi, Mater. Trans. **54**, 2173–2179 (2013)
48. A. Ashery, A.A.M. Farag, R. Mahani, Microelect. Eng. **87**, 2218–2224 (2010)
49. S. Altındal Yerişkin, J. Mater. Sci. **30**, 17032–17039 (2019)
50. S. Alptekin, S.O. Tan, S. Altindal, IEEE Trans. Nanotechnol. **18**, 1196–1199 (2019)
51. S. Altındal Yerişkin, Igdir Univ. J. Inst Sci. Technol. **9**, 835–846 (2019)
52. Y. Munikrishana Reddy, M.K. Nagaraj, M. Siva Pratap Reddy, J.-H. Lee, V. Rajagopal Reddy, Braz. J. Phys. **43**, 13–21 (2013)
53. M. Diale, F.D. Auret, Phys. B **404**, 4415–4418 (2009)